Myofibrillar Structural Variability Underlies Contractile Function in Stem Cell-Derived Cardiomyocytes

Kathryn Ufford, BS[1*]; Sabrina Friedline, BS[1*]; Zhaowen Tong[2], MS; Vi T. Tang, BS[1]; Amani S. Dobbs, BS[1]; Yao-Chang Tsan, PhD[1,3]; Stephanie L. Bielas, PhD[3,4]; Allen P. Liu, PhD[2,5-7]; Adam S. Helms, MD, MS[1]

1. Division of Cardiovascular Medicine, University of Michigan
2. Department of Biophysics, University of Michigan
3. Department of Human Genetics, University of Michigan
4. Department of Neuroscience, University of Michigan
5. Department of Mechanical Engineering, University of Michigan
6. Department of Biomedical Engineering, University of Michigan, Ann Arbor, Michigan, USA
7. Cellular and Molecular Biology Program, University of Michigan, Ann Arbor, Michigan, USA

*Contributed equally

Correspondence: adamhelm@umich.edu

Summary

Disease modeling and pharmaceutical testing using cardiomyocytes derived from induced pluripotent stem cell (iPSC-CMs) requires accurate assessment of contractile function. Micropatterning iPSC-CMs on elastic substrates controls cell shape and alignment to enable contractile studies, but the determinants of intrinsic variability in this system have been incompletely characterized. The primary objective of this study was to determine the impact of myofibrillar structure on contractile function in iPSC-CMs. After labeling micropatterned iPSC-CMs with a cell permeant F-actin dye, we imaged both myofibrillar structure and contractile function. Using automated myofibrillar image analysis, we demonstrate that myofibrillar abundance is widely variable among individual iPSC-CMs and strongly correlates with contractile function. This variability is not reduced by subcloning from single iPSCs to reduce genetic heterogeneity, persists with two different iPSC-CM purification methods, and similarly is present for embryonic stem cell-derived cardiomyocytes. This analysis provides compelling evidence that myofibrillar structure should be quantified and controlled for in studies investigating contractile function in iPSC-CMs.

Introduction

Cardiomyocytes derived from induced pluripotent stem cell (iPSC-CMs) have high potential as a model system for investigating causal mechanisms in cardiomyopathies and for pharmaceutical testing. Multiple approaches have been reported to assess contractile function in iPSC-CMs, including motion assessment in 2D monolayers, 3D microtissue approaches, and the single cell micropatterning approach, as recently reviewed.(Blair and Pruitt, 2020) While 2D monolayer motion analysis is simple, disorganized myofibrillar organization limits accuracy and reproducibility. In contrast, Ribeiro et al. demonstrated that the single iPSC-CM micropatterning approach has advantages of single cell precision and control over cell shape, which was shown to exert a large influence on contractile function.(Ribeiro et al., 2015) Additionally, the single cell iPSC-CM method avoids interactions with non-myocytes, which are generally admixed into 3D iPSC-CM microtissues to maintain tissue integrity but may increase the potential for batch-to-batch heterogeneity.(Thavandiran et al., 2013)

Yet, despite the advantages of single cell precision and geometric constraint, substantial variability has remained in the single micropatterned iPSC-CM system.(Helms et al., 2020; Ribeiro et al., 2015) Since the method is time intensive, the number of replicates has been limited in early studies, and, consequently, the extent of variability in contractile parameters has not been characterized. Here, we develop a novel technique to perform unbiased quantification of myofibrillar development in micropatterned iPSC-CMs using a live cell permeant dye that labels F-actin without requiring viral transduction or genetic engineering. Furthermore, using a large traction force microscopy (TFM) dataset of micropatterned iPSC-CMs, we construct a multivariable regression model that predicts contractile outputs from myofibrillar structural parameters. We present compelling evidence that variability in myofibrillar development is the key determinant of contractile function across individual iPSC-CMs. This variability is not due to genetic drift in heterogeneous stem cell populations, since it is not resolved by subcloning from single iPSCs; nor is this variability due to potential incomplete pluripotency in iPSCs,

since the same observations extend to embryonic stem cell-derived cardiomyocytes (ESC-CMs). These results have major implications for the use of iPSC-CMs for study of contractile function in disease modeling and pharmaceutical testing. Moreover, our findings emphasize the developmental variability present in stem cell-derived cardiomyocytes and the critical need for methods not only to improve maturation, but also to control for and minimize this heterogeneity.

Results

Microcontact printing achieves highly consistent single iPSC-CM geometries but variable contractile function.

To assess variability in micropatterned single iPSC-CMs, we selected the DF19-9-11 iPSC line (WiCell), a well-validated control cell line with similar calcium handling properties as other iPSC lines.(Hwang et al., 2015; Yu et al., 2009) We included iPSC-CMs purified by two alternative methods (selection by SIRPA membrane protein or metabolic selection with lactate-containing, glucose-deprived media) to assess any influence on contractile assays.(Dubois et al., 2011; Tohyama et al., 2013) On unpatterned substrates, lactate-selected iPSC-CMs were larger with greater aspect ratios than SIRPA-sorted iPSC-CMs, but both conditions had broad variance (**Figure 1A-B**). In contrast, micropatterned iPSC-CMs with either method exhibited similar size and aspect ratio (**Figure 1A-B**). We analyzed contractile phenotypes in these micropatterned iPSC-CMs on 8.7 kPa hydrogels, simulating physiologic elasticity, at day 32 (**Figure 1C**). Although shape and eccentricity influence single cell contractile function,(Bray et al., 2008; Ribeiro et al., 2015) we discovered that marked variability was still evident in contractile function (**Figure 1D**).

Micropatterned iPSC-CMs exhibit reproducible myofibrillar alignment but variable myofibrillar abundance.

The consistency and variability of myofibrillar development across large populations of micropatterned iPSC-CMs has not been reported but may underlie the variability in contractile function.

To characterize myofibrillar structure systematically, we performed sequential live imaging of F-actin using a cell permeant dye (SiR-actin) immediately following traction force microscopy to obtain near-simultaneous images (**Figure 2**). We then performed an unbiased quantification of myofibrillar structure using an automated pipeline developed in MATLAB that outputs measurements for the total cell area, aspect ratio, myofibrillar bundle area, density, alignment, and heterogeneity. Using this approach, we identified highly reproducible alignment of myofibrils but marked variability in myofibrillar structure across iPSC-CMs (**Figure 2A-D**). Micropatterned iPSC-CMs with even lesser quality myofibrillar development than in Figure 2D were also observed and generally exhibited non-uniform and very weak contractions – these cells were excluded (not represented in Figure 1 or subsequent analyses).

Myofibrillar structural parameters predict contractile function in micropatterned iPSC-CMs.

We hypothesized that the observed variability in contractile phenotypes is due to differential myofibrillar structure in individual iPSC-CMs. To test this hypothesis, we generated a dataset of traction force microscopy and myofibrillar structural measurements for 12 batches of control iPSC-CMs. With simple linear regression, only myofibrillar area significantly correlated with contractile force (**Figure 3A**, $R^2 = 0.32$, $p<0.0001$). While other structural parameters (as above) were not independently associated with contractile force, construction of a multivariable model of all structural parameters improved model prediction of contractile output (**Figure 3B**, $R^2 = 0.43$, $p<0.0001$ vs single variable regression). Only myofibrillar area was independently significantly associated with contractile force in the multivariable model ($p<0.0001$).

Calcium Transient Quantification but not Contraction Frequency Further Improves Multivariable Prediction of Contractile Function

Since higher contraction frequency correlates with calcium transient amplitudes and contractile force in the heart, we assessed whether spontaneous beating frequency of individual iPSC-CMs also contributes to variability of contractile phenotypes. No significant correlation was observed ($R^2 = 0.02$,

Figure 3C). This finding is likely due to the low contraction frequency of the iPSC-CMs in this study (75% <0.5 Hz, 96% <1.0 Hz), since the frequency-force response primarily exists at >1.0 Hz.(Endoh, 2004) Inclusion of contraction frequency in the multivariable model above did not improve the model fit (p=0.53).

To test whether residual variability in contractile function could be due to variability in calcium transients independent of contraction frequency, we quantified transient amplitudes using the fura-2 ratiometric calcium indicator in a subset. In simple linear regression, calcium transient amplitude did not correlate with contractile force (**Figure 3D**). However, inclusion of calcium transient amplitude in a multivariable analysis with myofibrillar area for this subset resulted in an improved model fit compared to regression with myofibrillar area alone (**Figure 3E**, R^2 = 0.60 vs. R^2 = 0.44, p=0.02). This result indicates that, while myofibrillar abundance most strongly correlates with contractile function, calcium handling additionally contributes to variability in contractile phenotypes across iPSC-CMs.

Myofibrillar structural parameters associate with batch variability in contractile function in micropatterned iPSC-CMs.

We next examined whether variability in myofibrillar abundance could be associated with batch-to-batch variability in contractile function. Linear regression of the mean values for each batch demonstrated that myofibrillar area strongly correlated with mean traction force for each batch (R^2 = 0.52, p<0.0001, **Figure 3F**). Control iPSC-CM batches consisted of 6 each from the DF19-9-11 control line and a single-cell derived subclone from this line (obtained as a non-targeted control line from a prior gene-editing experiment).(Helms et al., 2020) The purpose of including batches differentiated from this subclone was to determine whether genetic drift and heterogeneity during culture of the parent line could contribute to variability in myofibrillar and contractile phenotypes. We observed similar variability in both myofibrillar and contractile phenotypes in both the originating line (control A) and subclone (control B) iPSC-CMs across cells and batches (**Figure 2A, 2D**). This result indicates that variability in

myofibrillar and contractile phenotypes arise primarily from the differentiation environment and are not primarily due to genetic drift of individual iPSCs prior to differentiation. We also compared effects of iPSC-CM purification method by including 3 batches for each method for each control line. A similar relationship between myofibrillar abundance and contractile force was observed for each (**Figure 2A, 2D**).

Variability in Myofibrillar and Contractile Phenotypes Reduce Statistical Power and Increase Likelihood of False Positive Results from iPSC-CM Contractile Studies

To estimate the impact of contractile variability on iPSC-CM study design, we performed a power analysis using the standard deviation of traction forces in the control cell population (σ=487). To identify a 10% difference in maximum contractile force with β (type II error) = 0.9 and α (type I error) = 0.05 – the estimated necessary sample size is 974 cells for a 2-group comparison (487 cells per group), far surpassing the number of replicates in early studies using these techniques.

Although statistical tests generally used for iPSC-CM contractility studies assume an unbiased distribution of phenotypes across batches, batch-related bias is generally acknowledged as a limitation of iPSC-CM investigations. Since a practical number of batches (often 3) is typically chosen as representative, we assessed the potential for false positive results related to batch bias by comparing all possible combinations of comparison groups of 3 from the 6 SIRPA-purified control batches. We created artificial pooled groups of all possible 3 vs. 3 batch comparisons for a total of 10 possible comparisons. Out of these 10, 3 comparisons of contractile force were statistically significant by the independent samples t-test, consistent with a 30% false positive rate (**Figure 4A**). Normalization of contractile force by myofibrillar area prevented these false positives (**Figure 4B**). These results show that marked variability in contractile function across individual iPSC-CMs limits statistical power, while batch effect, if not controlled for, creates potential for false positive findings.

The myofibrillar area and contractile function relationship extends to embryonic stem cell-derived cardiomyocytes.

Although the DF19-9-11 iPSC line has been widely used and exhibits similar differentiated cardiomyocyte phenotypes as other control iPSC lines(Hwang et al., 2015), we further tested whether any potential incomplete pluripotency in the iPSC line could explain the variability in myofibrillar development by performing the same quantifications using an embryonic stem cell (ESC) line. Differentiated cardiomyocytes from the H9 ESC line (ESC-CMs) also exhibited marked variability in myofibrillar structure and function. As shown in **Figure 4C**, structure-function relationships for individual H9 ESC-CMs (green) distributed similarly as the population of iPSC-CMs (gray). Linear regression of myofibrillar area versus maximum contraction force revealed similar slopes for this relationship among both ESC-CMs and iPSC-CMs (**Figure 4C**).

Discussion

Micropatterning enables precise geometric control for single cell biomechanical studies. In this study, we used a technique that creates µm-level precision of adhesive protein deposition on polyacrylamide gels formulated for a physiologic workload. Similar to results with neonatal rat ventricular myocytes and initial reports in iPSC-CMs using similar techniques(Bray et al., 2008; Ribeiro et al., 2015), we found highly reproducible adherence of iPSC-CMs to micropatterns with induction of ~7:1 aspect ratios, simulating the shape of adult cardiomyocytes. Myofibers consistently aligned with the long axis of micropatterns, creating a tractable system for contractile quantification. Yet, despite robust induction of myocyte shape and myofibrillar alignment, unexpectedly large residual variability in iPSC-CM contractile function persisted. Our analysis reveals that this variability is in large part due to underlying variability of myofibrillar abundance across individual iPSC-CMs. Realization of the critical

influence of this variability on contractile measurements strongly suggests that myofibrillar structure should be measured and controlled for in studies investigating contractile function in iPSC-CMs.

The cause of variable myofibrillar development in micropatterned iPSC-CMs could be differential exogenous signaling cues in the preceding monolayer environment, heterogeneously stalled maturation, or variability in transcriptional activation of the myofibrillar development program. To reduce these factors, we implemented standardized protocols and purified iPSC-CMs using two different methods (SIRPA-purification or metabolic selection), both of which yielded similar results. We also replated iPSC-CMs as purified monolayers prior to seeding iPSC-CMs to micropatterns to reduce potential influence of non-myocytes in the original differentiated populations. Single iPSC-CMs were also maintained at a physiologic calcium level, which we found was essential to achieve robust contractile force, similar to another recent report.(Wheelwright et al., 2018) The persistence of variability despite the measures employed here likely indicates a fundamental stalling in maturation that is heterogeneous across populations of single iPSC-CMs. We found that a longer culture time (>32 days) did not result in a significant improvement in myofibrillar development or contractile force (not shown). Wheelwright et al. observed that most improvement in contractile function occurred from day 14 to day 30, with only a modest incremental improvement with extension to 90 days.(Wheelwright et al., 2018) Our findings are consistent with single cell RNA-seq analyses that demonstrated stalled and variable developmental profiles in iPSC-CMs differentiated with similar methods.(Friedman et al., 2018) Consequently, quantification of myofibrillar development enables verification of similar developmental state among comparison groups, and this approach was essential in our prior comparison across *MYBPC3* genotypes.(Helms et al., 2020) Here, we further increase the rigor of these comparisons by implementing an unbiased, automated myofibril quantification method and multiple linear regression. This technique can be used to reduce the sample size in iPSC-CM studies, since our power analysis indicated that, otherwise, the required sample size for adequately powered studies would be

impractically large. Additionally, our results indicate that controlling for the myofibrillar development state may be critical to avoid confounding from batch-related differences that might lead to false conclusions.

Myofibrillar structural parameters explained a large degree of the variability observed in contractile function, though substantial residual variability was not accounted for in the multiple regression model. One likely explanation for residual variability is that a 2-dimensional approach for quantifying myofibrillar abundance underestimates myofibrils in regions of high myofibrillar density due to a limited capacity to resolve superimposed structures. Z-stack imaging with standardized absolute intensity quantification would likely increase the accuracy of the regression model, but that approach would not have readily enabled imaging of contracting live cells as performed in this study. Additionally, we performed a linear regression based on the assumption that myofilament addition in parallel would be linearly related to contractile output. Actual intracellular relationships among myofilament organization and contractile output are likely more complex. Finally, contractile function may also vary due to cell-cell differences in transcriptional programs independent from myofibrillar development, such as variability in sarcomere gene transcript variant / isoform expression (e.g. TNNI3) and metabolic capacity (Birket et al., 2015; Correia et al., 2017; Wheelwright et al., 2020).

In conclusion, our results are compelling evidence that single micropatterned iPSC-CMs exhibit a vast degree of myofibrillar structural variability that underlies variability in contractile function. This variability is not controlled for by either of two standard purification methods or by subcloning to reduce genetic heterogeneity. Simultaneous imaging with an F-actin cell-permeant dye allows assessment of myofibrillar structure concurrent with contractile imaging, and the automated imaging analysis pipeline implemented here enables a multiple regression approach to rigorously quantify the effects of other variables on contractile function. Investigations of cardiomyocyte contractile function

using the iPSC-CM model should routinely employ methods to account for this variability. Moreover, future efforts should be directed toward reducing developmental variability in differentiated iPSC-CMs.

Experimental Procedures

Stem Cell and Cardiomyocyte Culture: Control iPSCs (DF19-9-11) and ESCs (H9 WA09) were obtained from WiCell. A series of subclones were derived from the originating iPSC line during a previously reported gene-editing experiment.(Helms et al., 2020) Cardiac differentiation, sarcomere gene expression, and sarcomere protein content were all similar among subclones, including those with *MYBPC3* variants (RNA-seq data for differentiated iPSC-CMs for each are available on the Gene Expression Omnibus server.(Helms et al., 2020) All iPSCs were cultured in mTeSR1 and differentiated using Wnt modulation.(Lian et al., 2012) iPSCs were verified free of mycoplasma using MycoAlertTM (Lonza). iPSC-CM were purified by either SIRPA-selection using magnetic beads at day 15 (Herron et al., 2016) or metabolic selection using glucose-deprived, lactate-containing media on days 12-16.(Burridge et al., 2015; Tohyama et al., 2013) Purified iPSC-CMs were first replated as monolayers until day 25, then replated to micropatterned substrates at 6000k/cm^2 density until assay at day 32. Because RPMI contains a subphysiologic level of calcium (0.4 mM), RPMI was blended 50:50 with DMEM (1.10 mM calcium) on day 1 following replating, and then 25:75 with DMEM (1.45 mM calcium) on day 3 following single cell replating (1X B27 supplement).

Microcontact Printing and Live-Cell Imaging: Single cell micropatterning was performed as described.(Helms et al., 2020) Briefly, a chrome mask with grids of 7:1 aspect ratio, 1750 µm^2 area rectangles was used to generate a silicon wafer with micropatterned spin-coated SU-8. PDMS stamps were molded with 10:1 (base:curing agent) Sylgard® 184 (Corning). Polyacrylamide hydrogels were fabricated onto glass coverslips and microprinted with fibronectin (Sigma).(Grevesse et al., 2013, 2014; Helms et al., 2020) Hydrogels contained 0.2 µm diameter FluoSpheresTM (Thermo Fisher). All iPSC-CMs were labeled for F-actin with the cell permeant dye, SiR-Actin (Cytoskeleton, Inc.), prior to imaging (0.5

μM, 1 hour) to enable visualization of myofibrils during contractile imaging. Medias were equilibrated (37 C and 5% CO_2) prior to media changes. Microscopy was performed at 37 C and 5% CO_2 to acquire videos of spontaneously contracting iPSC-CMs, the underlying layer of fluorescent microbeads, and myofibrils. Only iPSC-CMs exhibiting spontaneous contractions with both ends symmetrically contracting toward the center were included.

Image Processing: Traction force analysis was performed as described.(Han et al., 2015; Helms et al., 2020) Time-force data was exported to Microsoft Excel for curve fitting. Images of myofibrils were processed using custom scripts in MATLAB® that extract intensity-based signals for individual myofibrillar bundles by identification and merger of F-actin signal peaks connected along the long axis of the image. The algorithm then calculates the standard deviation for alignment of these myofibrillar bundles, total area of identified bundles, and indices of both short- and long-axis heterogeneity of the bundles.

Intracellular Calcium Quantification: iPSC-CMs were loaded with 1 μM fura-2 AM (Thermo Fisher) for 10 min, rinsed with 250 μM probenecid in HBSS for 5 min, changed to pre-equilibrated media, and then incubated for 30 min prior to imaging through a Nikon Super Fluor 40x objective. The emitted light intensity following alternating excitation at 340 nm and 380 nm was reported as fura-2 ratios.

Statistical Analysis: Continuous variables were compared by ANOVA with multiple testing correction. Linear regressions were performed with the least squares method. Goodness of fit was assessed by R^2, and models were compared with the extra-sum-of-squares F-test. All analyses were performed in GraphPad Prism.

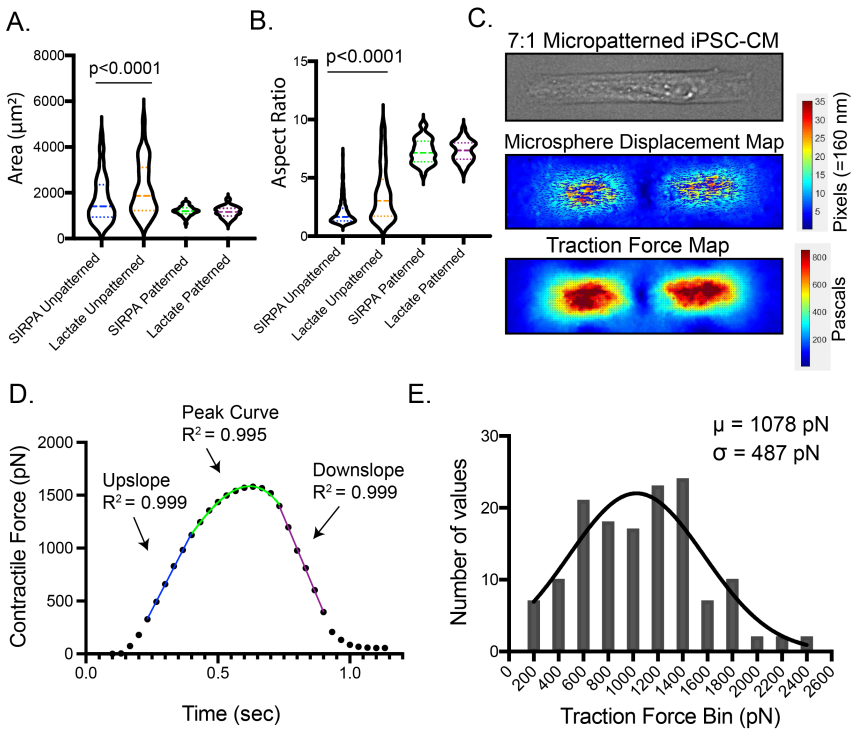

Figure 1. Microcontact printing achieves highly consistent single iPSC-CM geometries but variable contractile function. A-B. Size and aspect ratio of single iPSC-CMs both vary markedly with standard culture conditions but were reproducibly constrained with micropatterning (N=167 unpatterned SIRPA, N=121 unpatterned metabolic selection, N=53 micropatterned SIRPA, N=90 micropatterned metabolic selection, comparisons by ANOVA). **C.** Representative displacement and traction force maps are shown at peak contraction. Displacements of microbeads were tracked and resolved to a traction force map to calculate the whole-cell traction force at 30 msec intervals. **D.** Representative analysis of a contractile curve demonstrates that partitioning into 3 components enables curve fitting to the calculate contraction velocity (upslope fit with linear regression, blue, invariably with R^2>0.99), peak contraction (fit with polynomial, green, with typical R^2>0.98), and relaxation velocity (fit with linear regression, red, invariably with R^2>0.99). **E.** Histogram of maximum traction force across the population of individual micropatterned iPSC-CMs (N=143) demonstrates a Gaussian distribution with a standard deviation of 487 pN.

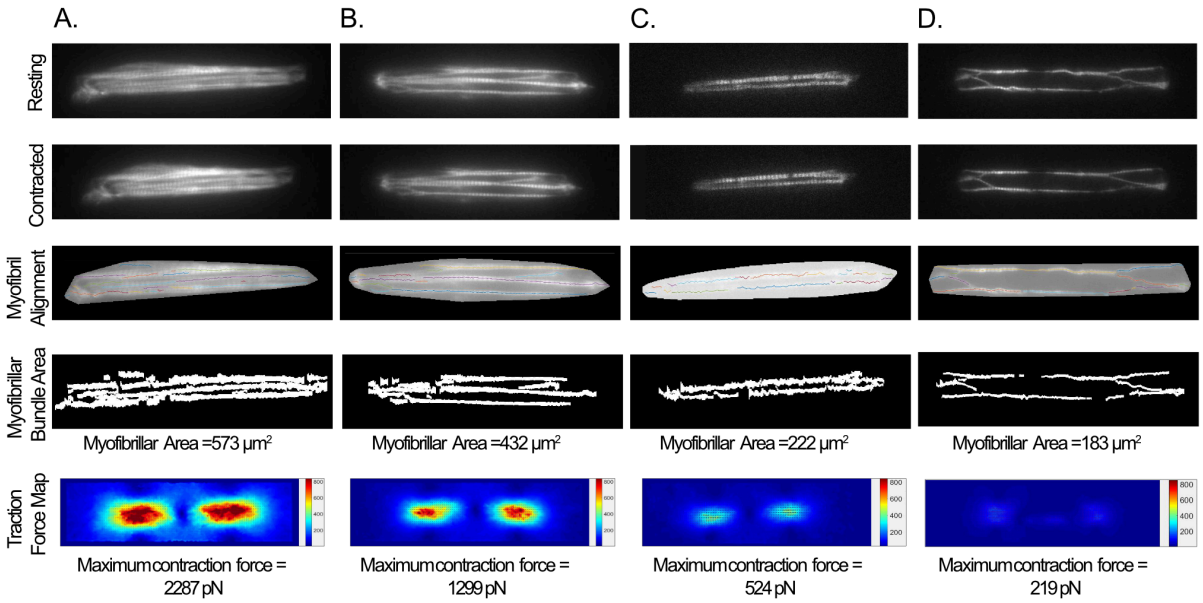

Figure 2. Single micropatterned iPSC-CMs demonstrate consistent myofibrillar alignment but variable myofibrillar structural development. A. Representative images of a micropatterned iPSC-CM with dense myofibrillar bundles (fluorescence imaging of F-actin) obtained at time of traction force microscopy. Time series of images of F-actin were collected throughout the contraction cycle to avoid blur (top row at rest; 2nd row at peak contraction). An automated image processing algorithm was used to extract a masked cell area and identify myofibrillar bundles. The algorithm calculates myofibrillar alignment (3rd row) and total myofibrillar bundle area (4th row), as well as heterogeneity in both short- and long-axis directions. A corresponding traction force map is shown in the 5th row. **B-D.** Representative images of micropatterned iPSC-CMs across a range of myofibrillar densities with corresponding traction force maps. Myofibrillar alignment was robust along the long axis for all iPSC-CMs, but contractile force was diminished in iPSC-CMs with low myofibrillar density (C-D).

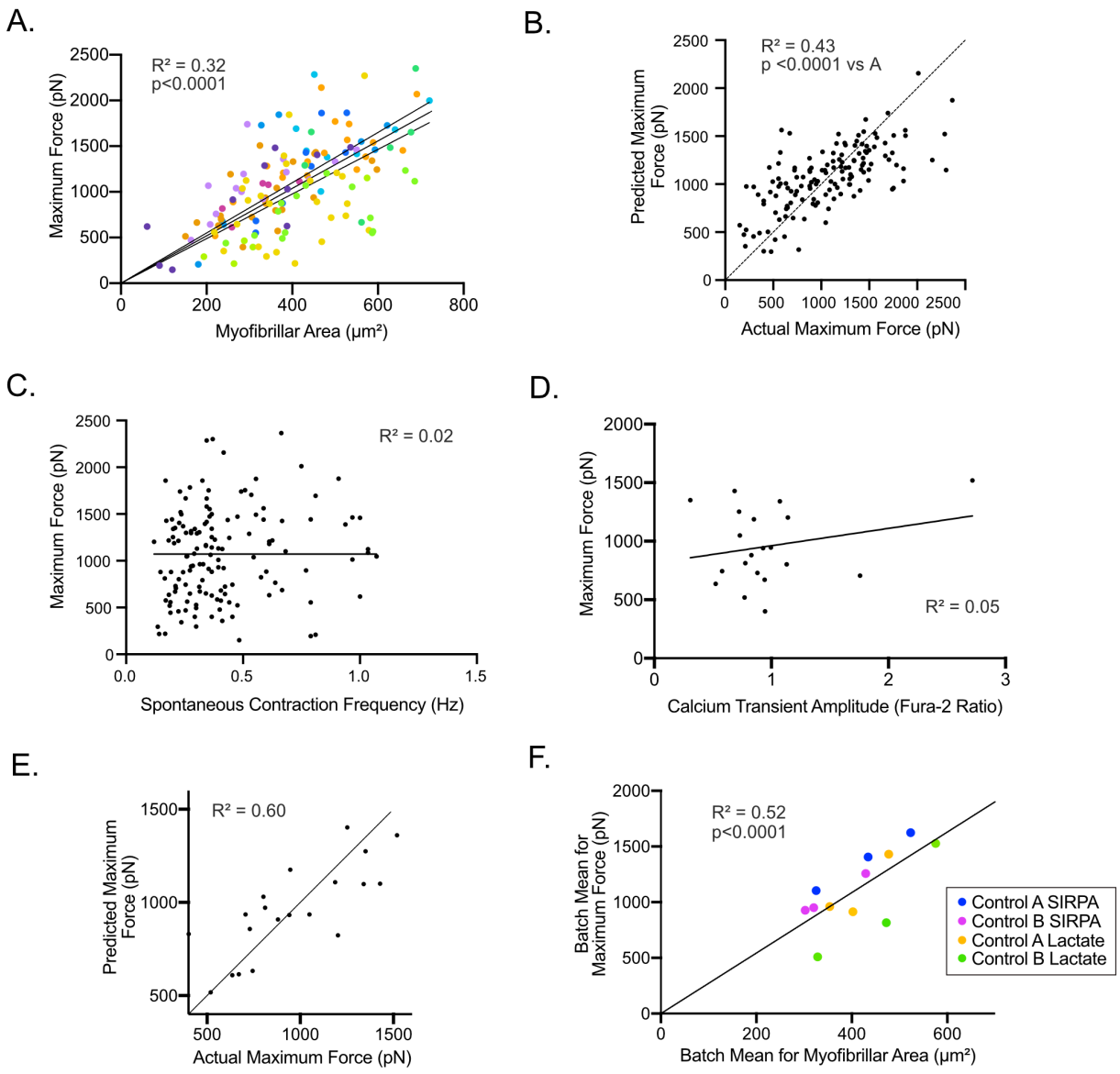

Figure 3. Myofibrillar structure correlates with maximal contraction force. A. Linear regression demonstrates a significantly positive correlation between myofibrillar area and maximum contraction force (N=143, p<0.0001 vs. slope of 0, trend line with 95% confidence interval regression lines shown). Each iPSC-CM batch is shown as a different color (shades of corresponding colors match batch colors in 2F). **B.** Actual versus predicted maximum traction force from multiple regression incorporating myofibrillar area, cell area, aspect ratio, and heterogeneity indices. The model fit is improved compared to the univariate linear regression in A. **C.** Spontaneous contraction frequency does not correlate with

contractile force. **D.** Calcium transient amplitudes did not correlate with contractile force with simple linear regression (N=20). **E.** Addition of calcium transient amplitudes to myofibrillar area in a multivariable model improved model fit (N=20, R^2 = 0.60 vs. R^2 = 0.44, p=0.02). **F.** Mean myofibrillar area per batch correlated with mean contractile force across control iPSC-CM batches for both control lines purified by either SIRPA sorting or metabolic selection. All model comparisons performed with the extra sum-of-squares F-test considering $p<0.05$ statistically significant.

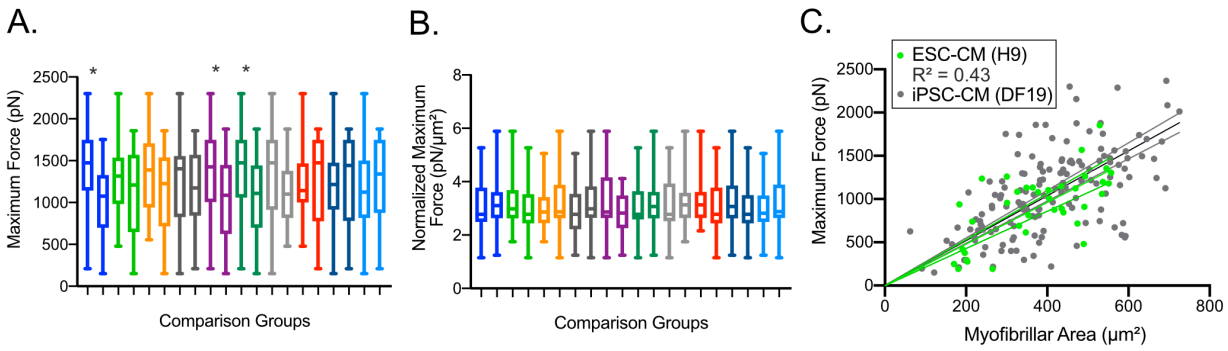

Figure 4. Myofibrillar variability leads to batch effect and is similarly present in embryonic stem cell-derived cardiomyocytes. A. The 6 control SIRPA-selected batches from Figure 3 were subdivided into all possible combinations of 3 batches vs. 3 batches to assess the influence of batch effect on statistical comparisons of contractile force. Each unique 2-group combination is shown in a different color and were compared using the independent samples t-test (box plot shows 75% interquartile with whiskers showing range; * indicates $p<0.05$). **B.** Normalization of contractile force by myofibrillar area results in a lack of statistical significant comparisons among the same groups as in A. **C.** Linear regression of myofibrillar area versus maximum contractile force for ESC-CMs (green points and regression line +/- 95% confidence intervals, N=37) demonstrated a similar relationship as for iPSC-CMs (gray points and regression line +/- 95% confidence intervals, N=143, same as in Figure 3A).

Acknowledgements

This work was funded by the NIH (K08HL130455 to ASH and R21GM134167 to APL) and NSF (CMMI-1561794 to APL). We thank Kevin Kit Parker and Thomas Grevesse for initial training in polyacrylamide gel micropatterning, Sangyoon Han for assistance in implementation of traction force analysis software, and Lap Man Lee for fabrication of the micropatterning wafer.

Author Contributions

Conceptualization - ASH, APL; Methodology - ASH, APL; Investigation - KU, SF, ZT, VTT, AD, YCT; Writing - ASH, KU; Writing, Review/Editing - ASH, APL, SLB; Funding – ASH, APL; Supervision – ASH, APL, SLB.

Declaration of Interests

The authors declare no competing interests.

References

Birket, M.J., Ribeiro, M.C., Kosmidis, G., Ward, D., Leitoguinho, A.R., van de Pol, V., Dambrot, C., Devalla, H.D., Davis, R.P., Mastroberardino, P.G., et al. (2015). Contractile Defect Caused by Mutation in MYBPC3 Revealed under Conditions Optimized for Human PSC-Cardiomyocyte Function. Cell Rep. *13*, 733–745.

Blair, C.A., and Pruitt, B.L. (2020). Mechanobiology Assays with Applications in Cardiomyocyte Biology and Cardiotoxicity. Adv. Healthc. Mater. *9*.

Bray, M.A., Sheehy, S.P., and Parker, K.K. (2008). Sarcomere alignment is regulated by myocyte shape. Cell Motil Cytoskelet. *65*, 641–651.

Burridge, P.W., Holmstrom, A., and Wu, J.C. (2015). Chemically Defined Culture and Cardiomyocyte Differentiation of Human Pluripotent Stem Cells. Curr Protoc Hum Genet. *87:21.3.1-*, 10.1002/0471142905.hg2103s87.

Correia, C., Koshkin, A., Duarte, P., Hu, D., Teixeira, A., Domian, I., Serra, M., and Alves, P.M. (2017). Distinct carbon sources affect structural and functional maturation of cardiomyocytes derived from human pluripotent stem cells. Sci. Rep. *7*.

Dubois, N.C., Craft, A.M., Sharma, P., Elliott, D.A., Stanley, E.G., Elefanty, A.G., Gramolini, A., and Keller, G. (2011). SIRPA is a specific cell-surface marker for isolating cardiomyocytes derived from human pluripotent stem cells. Nat. Biotechnol. *29*, 1011–1018.

Endoh, M. (2004). Force-frequency relationship in intact mammalian ventricular myocardium: Physiological and pathophysiological relevance. Eur. J. Pharmacol. *500*, 73–86.

Friedman, C.E., Nguyen, Q., Lukowski, S.W., Helfer, A., Chiu, H.S., Miklas, J., Levy, S., Suo, S., Han, J.D.J., Osteil, P., et al. (2018). Single-Cell Transcriptomic Analysis of Cardiac Differentiation from Human PSCs Reveals HOPX-Dependent Cardiomyocyte Maturation. Cell Stem Cell *23*, 586-598.e8.

Grevesse, T., Versaevel, M., Circelli, G., Desprez, S., and Gabriele, S. (2013). A simple route to functionalize polyacrylamide hydrogels for the independent tuning of mechanotransduction cues. Lab

Chip *13*, 777–780.

Grevesse, T., Versaevel, M., and Gabriele, S. (2014). Preparation of hydroxy-PAAm hydrogels for decoupling the effects of mechanotransduction cues. J. Vis. Exp.

Han, S.J., Oak, Y., Groisman, A., and Danuser, G. (2015). Traction microscopy to identify force modulation in subresolution adhesions. Nat Methods *12*, 653–656.

Helms, A.S., Tang, V.T., O'Leary, T.S., Friedline, S., Wauchope, M., Arora, A., Wasserman, A.H., Smith, E.D., Lee, L.M., Wen, X.W., et al. (2020). Effects of MYBPC3 loss-of-function mutations preceding hypertrophic cardiomyopathy. JCI Insight *5*.

Herron, T.J., Rocha, A.M., Campbell, K.F., Ponce-Balbuena, D., Willis, B.C., Guerrero-Serna, G., Liu, Q., Klos, M., Musa, H., Zarzoso, M., et al. (2016). Extracellular Matrix-Mediated Maturation of Human Pluripotent Stem Cell-Derived Cardiac Monolayer Structure and Electrophysiological Function. Circ Arrhythm Electrophysiol. *9*, e003638. doi: 10.1161/CIRCEP.113.003638.

Hwang, H.S., Kryshtal, D.O., Feaster, T.K., Sanchez-Freire, V., Zhang, J., Kamp, T.J., Hong, C.C., Wu, J.C., and Knollmann, B.C. (2015). Comparable calcium handling of human iPSC-derived cardiomyocytes generated by multiple laboratories. J Mol Cell Cardiol. *85:79-88.*, 10.1016/j.yjmcc.2015.05.003. Epub 2015 May 14.

Lian, X., Hsiao, C., Wilson, G., Zhu, K., Hazeltine, L.B., Azarin, S.M., Raval, K.K., Zhang, J., Kamp, T.J., and Palecek, S.P. (2012). Robust cardiomyocyte differentiation from human pluripotent stem cells via temporal modulation of canonical Wnt signaling. Proc. Natl. Acad. Sci. U. S. A. *109*, E1848–E1857.

Ribeiro, A.J., Ang, Y.S., Fu, J.D., Rivas, R.N., Mohamed, T.M., Higgs, G.C., Srivastava, D., and Pruitt, B.L. (2015). Contractility of single cardiomyocytes differentiated from pluripotent stem cells depends on physiological shape and substrate stiffness. Proc Natl Acad Sci U S A *112*, 12705–12710.

Thavandiran, N., Dubois, N., Mikryukov, A., Massé, S., Beca, B., Simmons, C.A., Deshpande, V.S., McGarry, J.P., Chen, C.S., Nanthakumar, K., et al. (2013). Design and formulation of functional

pluripotent stem cell-derived cardiac microtissues. Proc. Natl. Acad. Sci. U. S. A. *110*.

Tohyama, S., Hattori, F., Sano, M., Hishiki, T., Nagahata, Y., Matsuura, T., Hashimoto, H., Suzuki, T., Yamashita, H., Satoh, Y., et al. (2013). Distinct metabolic flow enables large-scale purification of mouse and human pluripotent stem cell-derived cardiomyocytes. Cell Stem Cell *12*, 127–137.

Wheelwright, M., Win, Z., Mikkila, J.L., Amen, K.Y., Alford, P.W., and Metzger, J.M. (2018). Investigation of human iPSC-derived cardiac myocyte functional maturation by single cell traction force microscopy. PLoS One *13*.

Wheelwright, M., Mikkila, J., Bedada, F.B., Mandegar, M.A., Thompson, B.R., and Metzger, J.M. (2020). Advancing physiological maturation in human iPSC-derived cardiac muscle by gene editing an inducible adult troponin isoform switch. Stem Cells.

Yu, J., Hu, K., Smuga-Otto, K., Tian, S., Stewart, R., Slukvin II, and Thomson, J.A. (2009). Human induced pluripotent stem cells free of vector and transgene sequences. Science (80-.). *324*, 797–801.